Electrical Impedance Tomography for Imaging Tissue Electroporation

Rafael V. Davalos*, David M. Otten, Lluis M. Mir, and Boris Rubinsky

***Abstract*—Electroporation is a method to introduce molecules, such as gene constructs or small drugs, into cells by temporarily permeating the cell membrane with electric pulses. In molecular medicine and biotechnology, tissue electroporation is performed with electrodes placed in the target area of the body. Currently, tissue electroporation, as with all other methods of molecular medicine, is performed without real-time control or near-term information regarding the extent and degree of electroporation. This paper expands the work from our previous study by implementing new *ex vivo* experimental data with "front-tracking" analysis for the image reconstruction algorithm. The experimental data is incorporated into numerical simulations of electroporation procedures and images are generated using the new reconstruction algorithm to demonstrate that electrical impedance tomography (EIT) can produce an image of the electroporated area. Combining EIT with electroporation could become an important biotechnological and medical technique to introduce therapeutic molecules into cells in tissue at predetermined areas of the body.**

***Index Terms*—Bioimpedance tomography, electrochemotherapy, electrogenetherapy, electropermeabilization, medical imaging.**

I. Introduction

MOLECULAR medicine often requires the introduction of specific molecules, such as gene constructs or (macro) molecular drugs, which normally cannot penetrate the cell membrane, into specifically targeted cells in the body. Among the methods to overcome this obstacle is tissue electroporation, also termed electropermeabilization [1], [2]. In tissue electroporation, electrodes are placed around or into the targeted tissue and electrical pulses are applied to permeabilize the cell membrane. For a specific set of pulse parameters (e.g. pulse number, frequency, duration, shape), the effect that the treatment has depends on the strength of the local electric field to which the cells are exposed [2], [3]. The treatment can result in either no change, reversible permeation (in which the cell membrane reseals), or irreversible permeation (i.e. cell death—in which the cell membrane does not reseal).

Currently, tissue electroporation, as with all other methods of molecular medicine, is performed without real-time or near-term control. In other words, there is no information during the procedure regarding the extent and degree of electroporation. Therefore, the only indication concerning the outcome of the treatment is long-term, such as the expression or lack of expression of a gene [4], the cure or lack of cure of the cancer in the animal or patient [5], [6], or the retention of radioactive tracers [2]–[4], [7].

Biological tissues contain extracellular and intracellular electrolytes, which are good conductors of electricity. During electroporation the cell membrane lipid bilayer, which is normally electrically insulating, becomes permeable to chemical species including electrolytes. Researchers have studied electroporation through detecting changes in membrane resistance with patch clamps [8], fluorescent markers [9], and current-voltage measurements. These current-voltage measurements have been conducted *in vitro* with cells in suspension [10] or with cells cultured directly on electrodes [11] as well as *ex vivo* before and after skin electroporation [12]. We also have shown earlier, in experiments with individual cells *in vitro* that the change in the electrical impedance of individual cells during electroporation is measurable and detectable [13].

Electrical impedance tomography (EIT) is an imaging method that maps the electrical impedance distribution inside the tissue. The procedure generally consists of surrounding the body or organ to be imaged with electrodes that inject current patterns through electrode pairs while the ensuing potentials are measured on the remaining electrodes. It should be noted that the electric fields generated during data acquisition for an EIT system are subsensory with magnitudes much lower than the fields required to induce electroporation and would not modify the extent of the electroporated volume. A reconstruction algorithm takes these voltage measurements, the current pair information, and electrode geometries as input to produce an image. Such an image should also reveal the extent of the electroporated area. This would help ensure that all of the cells in the target area will become penetrable to the treatment (macro) molecules without affecting the other cells in the surrounding region. However, since cells in tissue inside the body are surrounded by extracellular conductive fluid, it is not certain that the bulk properties of tissue will also change measurably during electroporation.

Our previous study demonstrated the potential for EIT to monitor electroporation by incorporating the conductivity change of a single cell during electroporation into an electrical model of the bulk tissue [14]. The present study combines new

Manuscript received April 19, 2003; revised July 25, 2003. This work was supported in part by the National Institutes of Health (NIH) under Grant 1 R21 RR15252-01. The work of R. Davalos was supported in part by Sandia National Laboratories. The work of L. M. Mir was supported in part by the CNRS, the Institut Gustave-Roussy, and the EU commission (QLK3-1999-00484 Cliniporator project). *Asterisk indicates corresponding author.*

*R. V. Davalos is with the Biomedical Engineering Laboratory, Department of Mechanical Engineering, 6178 Etcheverry Hall, University of California at Berkeley, Berkeley, CA 94720-1740 USA (e-mail: rvdaval@sandia.gov).

D. M. Otten and B. Rubinsky are with the Biomedical Engineering Laboratory, Department of Mechanical Engineering, 6178 Etcheverry Hall, University of California at Berkeley, Berkeley, CA 94720-1740 USA (e-mail: rubinsky@me.berkeley.edu).

L. M. Mir is with the Vectorology and gene transfer, UMR 8121 CNRS, Institut Gustave-Roussy, 39 rue Camille Desmoulins, F-94805 Villejuif Cédex, FRANCE (e-mail: luismir@igr.fr).

Digital Object Identifier 10.1109/TBME.2004.824148

0018-9294/04$20.00 © 2004 IEEE

experimental data from electroporation of liver tissue *ex vivo* and a new numerical model to further support our theory that electrical impedance tomography (EIT) can produce an image of the electroporated area. To investigate tissue electroporation in this study, we have designed a new experimental apparatus for *ex vivo* experiments to quantify the change in conductivity of rat liver during electroporation. We have also developed a special "front-tracking" EIT reconstruction algorithm, which is particularly suitable for imaging electroporation because it capitalizes on the fact that at low frequencies nonelectroporated cells have low conductivity. The experimental data is incorporated into numerical simulations of electroporation procedures and images are generated using the new reconstruction algorithm. The results reported here demonstrate that, during electroporation, the conductivity of tissue increases to an extent detectable using a typical EIT system.

II. Numerical Methods

To demonstrate the ability of EIT to image the extent of electroporation we developed two computer simulations. The first was of the process of electroporation in tissue and the second of the EIT imaging of this process. The first simulation uses a two-dimensional finite element model representing the liver containing a small section of tissue undergoing electroporation with boundary conditions based on standard electroporation electrode configurations. The electroporated area is determined by iteratively evaluating the electric field distribution in the model, updating the electrical properties of the elements inside the model as prescribed by the experimental results reported in this study. The result of these calculations is a conductivity map with five conductivity levels including four degrees of electroporation in the tissue. The EIT simulation uses this conductivity map as a virtual phantom for input to reconstruct an image of the electroporated area.

The numerical simulations were conducted on a Compaq Presario 1700 laptop computer with 256 MB of RAM and an 800 MHz processor using MATLAB's partial differential equation toolbox (The MathWorks, Inc. Natick, MA).

A. Electroporation Model

The electroporation simulation evaluates the potential and field distribution in the tissue due to an electrical pulse using a finite element model with ~6900 elements. To account for the change in electrical properties of the tissue during electroporation, the algorithm iteratively solves the Laplace equation [15]

$$\nabla \cdot (\sigma \nabla \phi) = 0 \tag{1}$$

where σ is the electrical conductivity and ϕ is the electrical potential. The surface of the analyzed tissue is assumed to be electrically isolated with a zero flux boundary condition, simulating that the organ is placed in an insulative fixture for imaging during the electroporation surgical procedure. The conductivity of the tissue is assumed to be initially at 0.13 S m^{-1}, which agrees with [16] at 1 kHz and was measured from one sample during the present experimental work. At locations where the electric field surpasses the values applied under our experimental conditions (i.e. 200, 300, 400 and 500 V/cm), the conductivity increases accordingly as prescribed by the experimental results. The electric fields are recalculated with the updated conductivity values until the solution converges. In order for the solution to converge, we assume that once the conductivity of an element increases, it will not revert to a lower value. This calculation provides the conductivity map of the electroporated tissue.

B. Reconstruction Model

1) Data Collection Algorithm: The input data for EIT are generally collected by surrounding the region to be imaged with electrodes, which inject subsensory sinusoidal currents through a series of electrode pairs ("projections") while recording the resulting voltages through the remaining electrodes. In our particular examples, 32 electrodes are equally spaced around the model periphery, and a 1-mA excitation current is injected through opposite electrode pairs while recording the remaining opposite electrode pair information. This is known as an "opposite-opposite" data collection algorithm [17]. This vector length defines the maximum number of independent variables (in our case, 464) for a well-defined matrix inverse to exist. For each current projection, the resulting voltages are obtained by solving the Poisson equation in a finely meshed finite-element system using the converged electroporated impedance distribution. The reconstruction algorithm produces an impedance image from these voltage measurements as well as the known current pair information and EIT electrode geometry data.

Measurement noise consistent with typical modern EIT systems (1.0% uniform probability distribution) was added to each electrode measurement [18]. It is assumed that the EIT electrodes in this case study are fixed in geometry, simulating a situation in which the liver is placed in an insulating, semi-rigid electrode array imaging fixture during a surgical procedure and, therefore, electrode placement uncertainty errors were not considered. For a general overview of EIT, see [19].

2) Reconstruction Algorithm: A vector of values representing physical properties within an image can describe any image. We will generically denote this property vector, which in some way represents our image, as $\boldsymbol{\alpha}$ (length n_α). The inverse problem then maps some set of independent voltage measurements, $\boldsymbol{V}_0$ (length n_V), to this image vector $\boldsymbol{\alpha}$.

The bulk of the calculations in most reconstruction algorithms can conceptually be broken into two main parts: one involving a solution to the forward problem, and the second being the construction of the Jacobian matrix. The forward problem solves, for a known impedance distribution, the measured surface voltages, $\boldsymbol{V}_{0\boldsymbol{m}}$, from the applied currents. The Jacobian matrix can be thought of as the differential change in each member of $\boldsymbol{V}_{0\boldsymbol{m}}$ given a small perturbation of each $\boldsymbol{\alpha}$.

3) Newton-Raphson Method: Of the numerous EIT reconstruction methods, we have chosen a modified Newton-Raphson method due to its excellent convergence properties [20]. This method attempts to iteratively minimize a cost function representing the overall voltage measurement differences between the simulated phantom and the reconstruction algorithm's internal model. Each successive iteration can be represented as

$$\alpha_{m+1} = \alpha_m + (f'^T f') f' (f - V_0) \tag{2}$$

where m is the iteration number, f is a function solving the forward problem ($f : \boldsymbol{\alpha} \rightarrow \boldsymbol{V}_{0\boldsymbol{m}}$) and f' is the n_V by n_α matrix derivative of the f function, i.e. a functional matrix with each entry representing the change in $\boldsymbol{V}_{0\boldsymbol{m}}$ given a fractional change in $\boldsymbol{\alpha}$. It is the job of the Newton-Raphson method to minimize

the difference between $\boldsymbol{V}_0$, the actual vector of voltage measurements collected from the EIT system, and $\boldsymbol{V}_{0\boldsymbol{m}}$, the vector obtained from the solution to the forward problem.

If the objective function is within some given tolerance, then $\boldsymbol{\alpha}$ represents an acceptable image and the iteration is terminated. If the objective function fails, determination of the next $\boldsymbol{\alpha}$ begins with the appropriate Jacobian calculation for each method. The new property vector is then found using (2). Any post-processing of the data is performed at this point before the cycle begins again at the forward solution using the new property vector.

The term f' in (2) refers to the Jacobian matrix of the forward solution and is an essential component of any Newton-Raphson algorithm. The Jacobian matrix needed for the Newton-Raphson method was calculated using a sensitivity matrix approach [21]. Marquardt regularization was used to overcome the ill-conditioning of the Jacobian matrix [22].

4) Front-Tracking Reconstruction Algorithm: The vast majority of reconstruction algorithms break the imaging region into a finite number of pixels where the values of $\boldsymbol{\alpha}$ would represent the impedance of each pixel. The reason behind this is that many imaging applications assume no prior knowledge of the physical impedance distribution within the imaging domain. In tumor detection, for instance, the radiologist is unaware of the possible tumor location or impedance contrast before imaging the target region. However, with electroporation there are many simplifying properties that would not be taken advantage of with pixel-based methods. This *a priori* knowledge includes knowledge of the electrical image of the tissue prior to electroporation, conductivity changes associated with electroporation, and the position of electroporation electrodes.

A family of techniques known as front-tracking methods [23] capitalizes on these properties. Instead of allowing the imaging region to have an arbitrary impedance distribution over the imaging domain, these techniques reconstruct the shape of a boundary with known interior and exterior impedances. Mathematically, rather than finding the impedance of each stationary image pixel, we divide the domain into a finite number of electrically homogeneous subregions defined by the boundaries, which are completely contained within the outer boundary.

These reconstruction algorithms adjust the shape of the inner region until the differences between the voltage measurements taken from the phantom and the ones from the imaging model are minimized. For our particular algorithm the boundary segment end positions are iteratively adjusted and $\boldsymbol{\alpha} = \boldsymbol{r}$, a vector of boundary segment end positions. A more detailed description of this algorithm is presented in [24]. This approach differs from proposed parametric methods [25] that adjust the overall shape properties (scaling, rotation, x-y translation, etc.).

The governing Laplace equation for each homogeneous region is written as

$$\nabla \cdot \nabla \phi = 0 \tag{3}$$

where ϕ is voltage. Continuity conditions are applied at each subregion boundary and the Neumann boundary condition is applied along the outer boundary. There are no Dirichlet (specified potential) boundary conditions since the outer boundary is insulative, but an artificial reference voltage is used in practice to make the system of equations solvable. In addition to making segmentation unnecessary, the front-tracking method can be solved using the more computationally efficient and more appropriate boundary element method (BEM) for the forward problem.

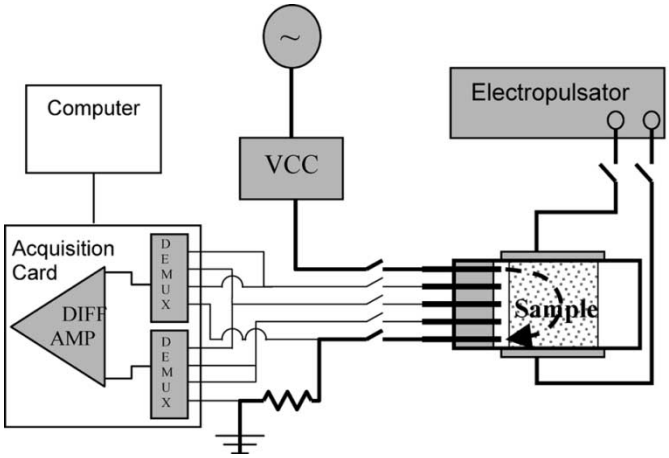

Fig. 1. Schematic of electrical apparatus.

III. Experimental Methods

To quantify the impedance change of tissue undergoing electroporation, we designed a simple single-frequency bio-impedance measurement system for rectangular tissue slices. The experimental apparatus is shown in Fig. 1. For each experiment, the tissue was placed onto a glass microscope slide surrounded by electrodes. The configuration consists of two separate sets of electrodes: one to administer the electroporation pulses and the other for detection. There is one switch to disengage the measurement electrodes and another to engage the electroporation electrodes to prevent the systems from interfering with each other.

A. Sample Preparation

Male Wistar rats of 200 g were anesthetized and sacrificed. After ventral laparotomy, livers were excised and sliced into rectangular pieces using a scalpel, approximately 2.5 cm in length, 1–2 cm in width and 0.2–0.4 cm in thickness. Experiments were conducted within 90 min from animal sacrifice with the tissue stored in 0.9% NaCl at room temperature until use. Size of sample, lag from time of sacrifice to data acquisition, and all voltage parameters were recorded for each sample. Liver tissue was chosen because it is macroscopically isotropic and, therefore, relatively homogenous, which eliminates any issues with the orientation of the electrodes with respect to the tissue. Also, there are no contractions during *in vivo* reversible electroporation with this organ, and at this stage we preferred not to deal with corrections required for these contractions. It should be noted that although only this type of tissue was used for the experiments, other samples could have as easily been used with this device.

B. Experimental Setup

The impedance change was measured with a 2.5 kHz, 0.3-mA rms sinusoidal current for 5 s, taken 10 s after the electroporation pulse. It was shown in earlier studies that permeability in tissues persists for periods longer than 15 s after delivery of the

pulses [2], [4], [26]. For the bioimpedance analysis, there are five 0.7-mm-wide square stainless-steel rods equally spaced at 4.5 mm, center-to-center, attached to one end of the slide with epoxy. A sinusoidal current is injected from the first electrode through the sample and out the last electrode. Its path, shown as a heavy solid line, is produced from the design in Fig. 1. These outer electrodes act as a permanent source/sink injection pair and the three electrodes in between are used for measurements. The system is designed to continuously record the root mean square of the voltage differential for all three possible combinations of measuring electrode pairs, sampling at 12 kHz. The three center electrodes enable one to measure the potential between any of the three combinations at any given time. The current through the system was determined by measuring the voltage drop across a 2-kΩ resistor located between the last electrode and ground.

To generate this current, a function generator (Tektronix FG502) creates a sinusoidal reference waveform used as input to a dual-op-amp (JFET TLO82CP) voltage-to-current converter (VCC), which is powered by a Raytheon (864 107-4) 25-V power supply. The system is controlled with a National Instruments DAQCard 700 data acquisition card (2.5-mV resolution) and a Compaq Presario 1700 notebook computer with 256 MB of RAM with an 800 MHz processor. The acquisition software was written using Lab Windows CVI 5.0 (National Instruments, Austin, TX).

C. Tissue Electroporation Experiments

The electroporation system is designed to supply eight square wave pulses up to 500 V cm^{-1} across the length of the tissue. Two parallel stainless-steel plate electrodes were placed along the width of the slide to apply the electric pulses. Conductive paste was applied between these electrodes and the tissue to ensure good electrical contact. The electroporation pulses were generated using a Jouan PS-15 square wave electropulsator (Jouan, St Herblain, France). An oscilloscope was attached to the system to verify delivery of the electric pulses. Eight 10-ms pulses at a frequency of 1 Hz were delivered for electric fields of 0, 200, 300, 400, and 500 V cm^{-1}. Three trials were performed for each gradient for a total of 15 experiments.

We assumed that the applied electric field from the plate electrodes uniformly electroporates the tissue. Therefore, since the injected current frequency is low, the change in the electrical conductivity of the tissue can be calculated with Ohm's Law by measuring the change in the potential drop across the electrodes and the injection current.

IV. Results

A simplified two-dimensional isotropic cross-section of a liver 7 cm in diameter is used for the simulation. The surface of the analyzed tissue is assumed to be electrically isolated with a zero flux boundary condition to simulate a situation in which the liver is temporarily placed in an insulating, semi-rigid 32-electrode array fixture for imaging during the electroporation surgical procedure.

A. Experimental Results for Forward Model

A summary of the experimental results with mean and standard deviation is included in Fig. 2. The results agree with *in vivo* studies on rat hind muscle, which showed a drop in the normalized resistivity associated with electrical shock trauma [27]. For input into our electroporation model the mean values of the conductivity changes at 0, 200, 300, 400, and 500 V/cm are used. The threshold gradient required to induce electroporation is taken from our experimental data to be 200 V cm^{-1} for pulses of 10-ms duration.

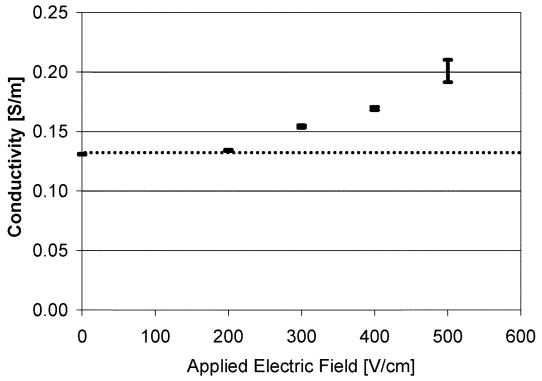

Fig. 2. Experimental data showing tissue conductivity change as a function of the electric field.

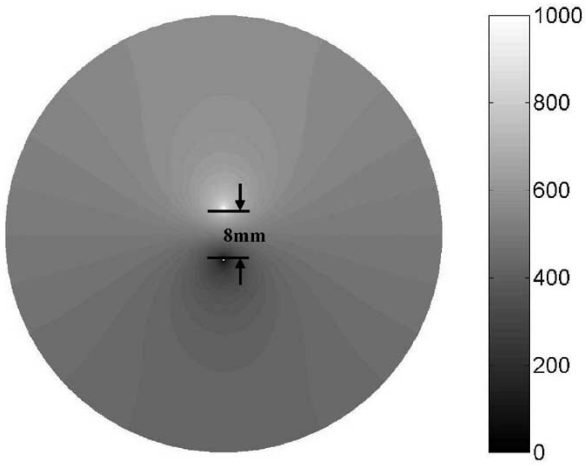

Fig. 3. Potential distribution and general schematic for first example (7 cm tissue; two 1.1-mm electrodes; 8 mm apart edge-to-edge no flux exterior; 1000 V/0 V).

B. Reconstruction Model

Our reconstruction algorithm consists of a 116 element mesh with 96 peripheral elements and 20 elements defining the electroporated area. The outer region maintains a conductivity of 0.13 S m^{-1} while the inner region uses a weighted conductivity value of 0.2 S m^{-1}. The algorithm initially assumes the electroporated region to be a circle with a 6-mm radius centered between the electroporation electrodes. The boundary conditions are zero flux for periphery segments except for the electrode source and sink. The EIT electrode element widths were 1 mm, and the source/sink current was $+/-1$ mA. The convergence criteria of the reconstruction algorithm were typically met after 10 iterations, taking approximately 90 min.

C. Reconstruction Examples

The liver tissue model was studied using two electroporation electrode geometrical configurations, which are examples of *in vivo* electroporation experiments conducted on rabbit liver [28], and murine skeletal muscle [3]. The first configuration (Fig. 3)

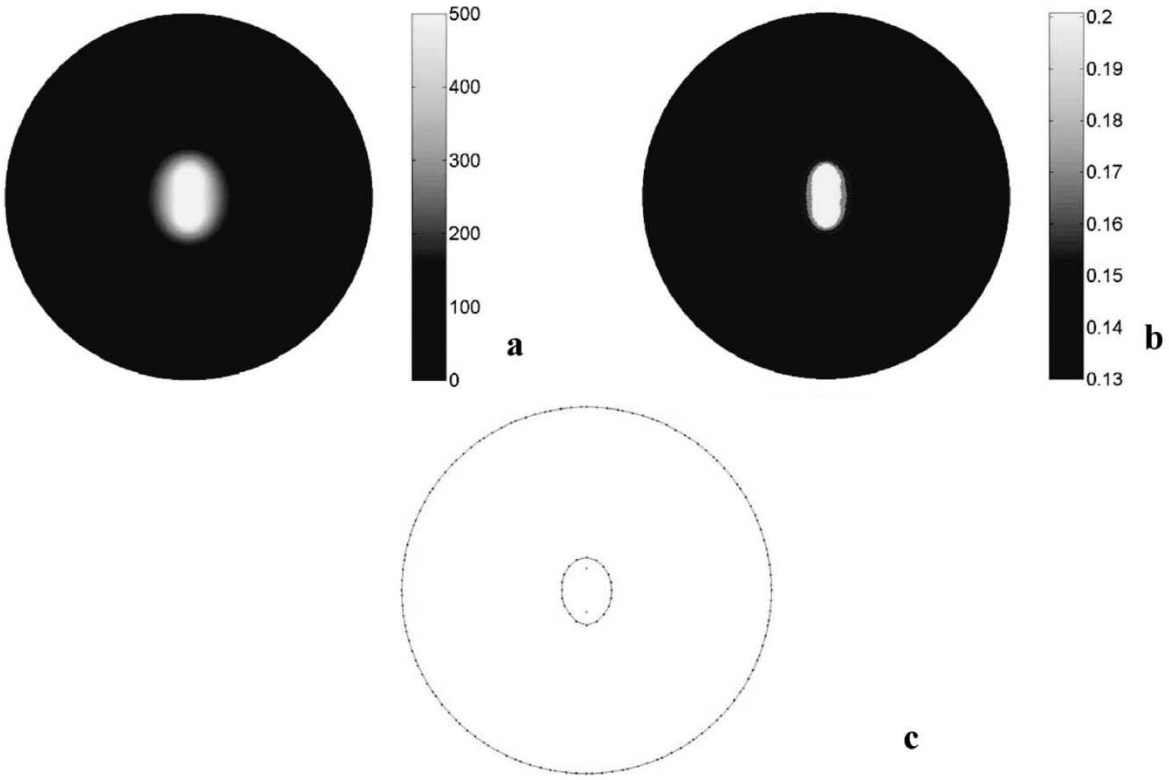

Fig. 4. Selected steps for first example (a) Electric field distribution [V/cm] (b) Conductivity map [S/m]. The light area indicates electroporated tissue. (c) Generated image.

has two electrodes separated with an inner distance of 8 mm, centered in the liver with one electrode at 1000 V and the other grounded. The second configuration has two rows of four electrodes centered in the liver. The center-to-center distance between the two rows is 4 mm, and the center-to-center spacing between the electrodes in each row is 2 mm. The voltage of the top row is set to 1200 V and the bottom row to ground. The diameters of the electrodes for the two examples are 1.1 and 0.5 mm, respectively.

Fig. 3 shows the potential distribution and labels the relevant dimensions and boundary conditions for the first configuration. Fig. 4(a)–(c) depicts selected modeling and imaging steps in our simulation for this configuration. Fig. 4(a) is the converged solution for the gradient distribution. For elements above a threshold gradient, the conductivity is increased to our measured value. Fig. 4(b) is the conductivity map generated using the information from Fig. 4(a). This distribution is then passed to the EIT imaging module, and Fig. 4(c) shows the generated image. Fig. 5(a), (b), and (c), respectively, shows the gradient distribution, conductivity map, and the generated image for the second example.

V. Discussion

The results in Figs. 4 and 5 have been obtained using realistic experimental data and demonstrate that EIT can produce an excellent image of the area affected by electroporation. The two examples were placed in the center of the tissue because this is a difficult location to image since conductivity perturbations at this location would minimally affect the surface voltage measurements and any other location would result in a larger signal to noise ratio. The obtained images further suggest that this new reconstruction algorithm may be more suitable for this application than the pixel-based method employed in our previous study because of its ability to incorporate the *a priori* information.

The clinical difficulties and the practicality of using EIT to image the extent of electroporation is identical to that of using EIT for imaging tissue in general, and the methodology for application is identical. In practical applications there is no need for assumptions of homogeneity—as the EIT system images nonhomogeneous tissues. Electroporation will produce a difference in impedance and this can be readily detected as a change in local impedance. Furthermore, we anticipate that imaging before and after electroporation could be used in a differential mode, which will single out only the electroporated area. However, in experiments with living animals, the differential mode would only work if a muscle relaxant was administered to ensure that the body did not spasm during the electroporation procedure. We anticipate that in the future, existing EIT systems for imaging tissue would also be useful for imaging electroporation without additional difficulties to clinical practice.

Before this method becomes a clinical technique, these results must be reproduced and verified using an actual EIT system to image physical phantoms, *ex vivo* tissue samples, and eventually electroporation *in vivo*. Future studies will need to more rigorously measure the performance of the system to noise, conductivity ratios, perturbation size and shape, number of EIT electrodes, and domain size. The resulting image will need to be evaluated in terms of visibility, sensitivity, spatial and conductivity resolution, contrast, and distinguishability. Complexities that have been ignored in this preliminary study may have to be

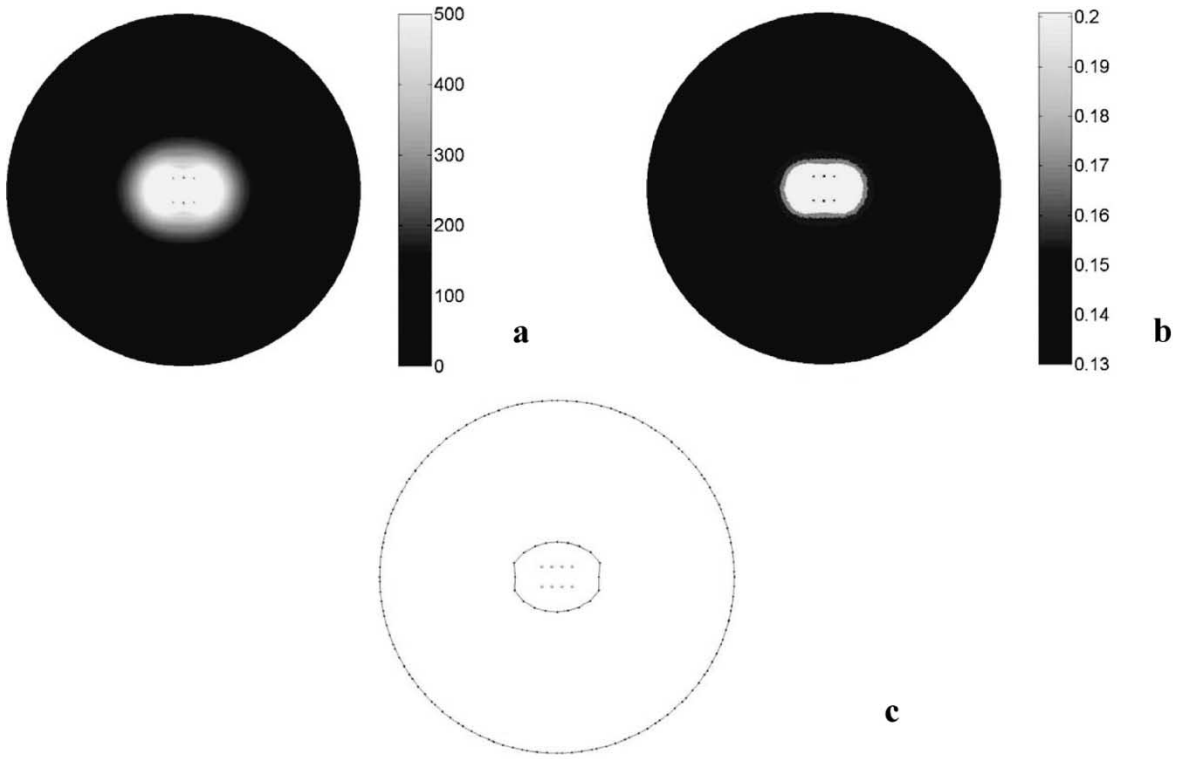

Fig. 5. Selected steps for second example (7 cm tissue; 0.5-mm electrodes; two rows 4 mm apart of four electrodes with 2-mm spacing; 1200 V top row, 0 V bottom row) (a) Electric field distribution [V/cm] (b) Conductivity map [S/m]. The light area indicates electroporated tissue. (c) Generated image.

addressed at that stage. These include inhomogeneities in real world liver samples from large blood vessels, nonplanar currents in 3D regions, and nonlinear electrode behavior. These issues should be resolvable through further reconstruction algorithm refinements. A promising enhancement particular to this application would incorporate the interior electroporation electrodes as EIT measurement points immediately after pulse delivery. These local voltage measurements could help resolve more precise images than the peripheral measurements alone.

In summary, in electroporation, as in all the other molecular medicine techniques, there is no method to actively monitor or control the process neither in real-time nor soon after the treatment, i.e. to determine during the procedure that the cell membranes have become temporarily permeabilized in the desired area of the tissue. This study demonstrates that rapid monitoring of novel electroporation-based therapies *in vivo* can be achieved through the synthesis of two fairly well understood techniques, electroporation and EIT.

REFERENCES

[1] J. C. Weaver, "Electroporation of cells and tissues," *IEEE Trans. Plasma Sci.*, vol. 28, pp. 24–33, Feb. 2000.

[2] L. M. Mir, "Therapeutic perspectives of *in vivo* cell electropermeabilization," *Bioelectrochem.*, vol. 53, pp. 1–10, 2001.

[3] J. Gehl, T. H. Sorensen, K. Nielsen, P. Raskmark, S. L. Nielsen, T. Skovsgaard, and L. M. Mir, "*In vivo* electroporation of skeletal muscle: Threshold, efficacy and relation to electric field distribution," *Biochim. Biophys. Acta.*, vol. 1428, pp. 223–240, 1999.

[4] L. M. Mir, M. F. Bureau, J. Gehl, R. Rangara, D. Rouy, J. Caillaud, P. Delaere, D. Branellec, B. Schartz, and D. Scherman, "High-efficiency gene transfer into skeletal muscle mediated by electric pulses," *Proc. Nat. Acad. Sci. USA*, vol. 96, pp. 4262–4267, 1999.

[5] L. M. Mir, L. F. Glass, G. Sersa, J. Teissie, C. Domenge, D. Miklavcic, M. J. Jaroszeski, S. Orlowski, D. S. Reintgen, Z. Rudolf, M. Belehradek, R. Gilbert, M. P. Rols, J. Belehradek, J. M. Bachaud, R. Deconti, B. Stabuc, M. Cemazar, P. Coninx, and R. Heller, "Effective treatment of cutaneous and subcutaneous malignant tumours by electrochemotherapy," *Br. J. Cancer*, vol. 77, pp. 2336–2342, 1998.

[6] R. Heller, "Treatment of cutaneous nodules using electrochemotherapy," *J. Florida Med. Assoc.*, vol. 82, pp. 147–150, 1995.

[7] J. Gehl and L. M. Mir, "Determination of optimal parameters for *in vivo* gene transfer using a rapid *in vivo* test for cell permeabilization," *Biochem. Biophys. Res. Commun.*, vol. 261, pp. 377–380, 1999.

[8] L. V. Chernomordik, S. I. Sukharev, S. V. Popov, V. F. Pastushenki, A. V. Sokirko, I. G. Abidor, and Y. A. Chizmadzhev, "The electrical breakdown of cell and lipid membranes: The similarity of phenomologies," *Biochim. Biophys. Acta.*, vol. 902, pp. 360–373, 1987.

[9] M. Hibino, M. Shigemori, H. Itoh, K. Nagayama, and K. Kinosita, "Membrane conductance of an electroporated cell analyzed by submicrosecond imaging of transmembrane potential," *Biophys. J.*, vol. 59, pp. 209–220, 1991.

[10] F. Pliquett and S. Wunderlich, "Relationship between cell parameters and pulse deformation due to these cells as well as its change after electrically induced membrane breakdown," *Bioelectrochem. Bioenergetics*, vol. 10, pp. 467–475, 1980.

[11] P. M. Ghosh, C. R. Keese, and I. Giaever, "Monitoring electropermeabilization in the plasma membrane of adherent mammalian cells," *Biophys. J.*, vol. 64, pp. 1602–1609, 1993.

[12] R. Vanbever, U. F. Pliquett, V. Preat, and J. C. Weaver, "Comparison of the effects of short, high-voltage and long, medium voltage pulses on skin electrical and transport properties," *J. Controlled Release*, vol. 69, pp. 35–47, 1999.

[13] Y. Huang and B. Rubinsky, "Micro-electroporation: Improving the efficiency and understanding of electrical permeabilization of cells," *Biomed. Microdevices*, vol. 2, pp. 145–150, 1999.

[14] R. V. Davalos, B. Rubinsky, and D. M. Otten, "A feasibility study for electrical impedance tomography as a means to monitor tissue electroporation for molecular medicine," *IEEE Trans. Biomed. Eng.*, vol. 49, pp. 400–403, Apr. 2002.

[15] R. Davalos, B. Rubinsky, and Y. Huang, "Electroporation: Bio-electrochemical mass transfer at the nano scale," *Microscale Thermophys. Eng.*, vol. 4, pp. 147–159, 2000.

[16] J. D. Bronzino, *The Biomedical Engineering Handbook*, 2nd ed. Boca Raton, FL: CRC, 2000, vol. 1.
[17] B. Rigaud and J. P. Morucci, "Bioelectrical impedance techniques in medicine—pt. III: Impedance imaging: First section: General concepts and hardware," *Crit. Rev. Biomed. Eng.*, vol. 24, pp. 467–597, 1996.
[18] W. Wang, M. Tang, M. McCormick, and X. Dong, "Preliminary results from an EIT breast imaging simulation system," *Physiol. Meas.*, vol. 22, pp. 39–48, 2001.
[19] K. Boone, D. Barber, and B. Brown, "Review—imaging with electricity: Report of the European concerted action on impedance tomography," *J. Med. Eng. Technol.*, vol. 21, pp. 201–232, 1997.
[20] T. J. Yorkey and J. G. Webster, "A comparison of impedance tomographic reconstruction algorithms," *Clin. Phys. Physiol. Meas.*, vol. 8, pp. 55–62, 1987.
[21] N. G. Gencer, Y. Z. Ider, and S. J. Williamson, "Electrical impedance tomography: Induced-current imaging achieved with a multiple coil system," *IEEE Trans. Biomed. Eng.*, vol. 43, pp. 139–149, Feb. 1996.
[22] D. W. Marquardt, "An algorithm for least-squares estimation of nonlinear parameters," *J. Appl. Math.*, vol. 11, pp. 431–441, 1963.
[23] H. L. Tsai and B. Rubinsky, "A numerical study using 'front tracking' finite elements on the morphological stability during transient solidification processes," *J. Crystal Growth*, vol. 69, pp. 29–46, 1984.
[24] D. M. Otten, "Cryosurgical monitoring using visible light imaging and electrical impedance tomograph—A feasibility study," Ph.D dissertation, University of California, Berkeley, 2000.
[25] J. C. de Munck, T. J. Faes, and R. M. Heethaar, "The boundary element method in the forward and inverse problem of electrical impedance tomography," *IEEE Trans. Biomed. Eng.*, vol. 47, pp. 792–800, June 2000.
[26] J. Gehl, T. Skovsgaard, and L. M. Mir, "Vascular reactions to *in vivo* electroporation: Characterization and consequences for drug and gene delivery," *Biochim. Biophys. Acta.*, vol. 1569, pp. 51–58, 2002.
[27] R. C. Lee, D. Zhang, and J. Hannig, "Biophysical injury mechanisms in electrical shock trauma," in *Ann. Rev. Biomed. Eng.*, M. L. Yarmish, K. R. Diller, and M. Toner, Eds. Palo Alto, CA: Ann. Rev. Press, 2000, vol. 2, pp. 477–509.
[28] D. Miklavcic, D. Semrov, H. Mekid, and L. M. Mir, "A validated model of *in vivo* electric field distribution in tissues for electrochemotherapy and for DNA electrotransfer for gene therapy," *Biochim. Biophys. Acta.*, vol. 1523, pp. 73–83, 2000.

Rafael V. Davalos was born in Bethesda, MD, in 1972. He received the B.S. degree in mechanical engineering from Cornell University, Ithaca, NY, in 1994 and M.S. in mechanical engineering in 1995 from the University of California, Berkeley. He completed the Ph.D. degree in bioengineering from the Department of Mechanical Engineering at the University of California, Berkeley, in 2002.

He is currently a Senior Engineer in the Microsystems Division at Sandia National Laboratories, Livermore, CA. His main research interests lie in feedback control mechanisms for molecular medicine, medical imaging, *in vivo* and *in vitro* cell electrical manipulation, BioMEMS and Microsystems.

David M. Otten was born in Denver, CO, in 1971. He received the B.S. degree from the University of Colorado at Boulder in 1993, and the Ph.D. degree in mechanical engineering, with an emphasis on control systems and bioengineering, from the University of California at Berkeley in 2000.

His graduate research interests have focused on minimally invasive surgical devices and feedback mechanisms including optical imaging and electrical impedance tomography for use with cryosurgical monitoring, optical tissue recognition, and cryosurgery-specific imaging reconstruction algorithms.

Lluis M. Mir was born in 1954 in Barcelona, Spain. He received his higher education from the Ecole Normale Supérieure de Paris (1974–1978), including the B.S. from University of Paris VI in 1976. He received the D.Sc. degree from the University of Toulouse, France, Toulouse, in 1983.

He joined the C.N.R.S. in 1978 and is currently the Director of Research at the Laboratory of Vectorology and Gene Transfer (UMR 8121, the Institute Gustave-Roussy and the University of Paris XI) in Villejuif, France. His main research interests lie in membrane electropermeabilization, specifically for the transfer of antitumor drugs and the electrotransfer of genes.

Boris Rubinsky received the Ph.D.degree from Massachusetts Institute of Technology, Cambridge, in 1980. His thesis research was in the area of bioengineering.

He is a Professor at the University of California, Berkeley, since 1980. During his career, he has developed several areas of research in bioengineering, including the field of imaging monitored cryosurgery and studies on cold tolerant and freezing tolerant animals. He has published over 200 research articles.